High integrin $\alpha_V\beta_6$ affinity reached by hybrid domain deletion slows ligand-binding on-rate

Xianchi Dong[a,1], Bo Zhao[a,1], Fu-Yang Lin[b], Chafen Lu[a], Bruce N. Rogers[b], and Timothy A. Springer[a,2]

[a]Children's Hospital Boston and Department of Biological Chemistry and Molecular Pharmacology, Harvard Medical School, Boston, MA 02115; and [b]Morphic Therapeutic, Waltham, MA 02451

Contributed by Timothy A. Springer, December 13, 2017 (sent for review October 27, 2017; reviewed by Dean Sheppard, Junichi Takagi, and Wendy E. E. Thomas)

The role of the hybrid domain in integrin affinity regulation is unknown, as is whether the kinetics of ligand binding is modulated by integrin affinity state. Here, we compare cell surface and soluble integrin $\alpha_V\beta_6$ truncation mutants for ligand-binding affinity, kinetics, and thermodynamics. Removal of the integrin transmembrane/cytoplasmic domains or lower legs has little effect on $\alpha_V\beta_6$ affinity, in contrast to β_1 integrins. In integrin opening, rearrangement at the interface between the βI and hybrid domains is linked to remodeling at the ligand-binding site at the opposite end of the βI domain, which greatly increases in affinity in the open conformation. The larger size of the βI-hybrid interface in the closed state suggests that the hybrid domain stabilizes closing. In agreement, deletion of the hybrid domain raised affinity by 50-fold. Surface plasmon resonance and isothermal titration calorimetry gave similar results and the latter revealed tradeoffs between enthalpy and entropy not apparent from affinity. At extremely high affinity reached in Mn^{2+} with hybrid domain truncation, $\alpha_V\beta_6$ on-rate for both pro-TGF-β1 and fibronectin declined. The results suggest that the open conformation of $\alpha_V\beta_6$ has lower on-rate than the closed conformation, correlate with constriction of the ligand-binding pocket in open $\alpha_V\beta_6$ structures, and suggest that the extended-closed conformation is kinetically selected for ligand binding. Subsequent transition to the extended-open conformation is stabilized by its much higher affinity for ligand and would also be stabilized by force exerted across ligand-bound integrins by the actin cytoskeleton.

integrin | TGF-β | affinity

Integrins, a family of cell-surface receptors, are a major class of adhesion molecules that link ligands to the cytoskeleton and mediate cellular migration and communication (1). Integrins feature large, multidomain structures. Integrin activation, namely increased binding affinity for ligand, is regulated by two types of conformational change: lower leg extension and hybrid domain swing-out (Fig. 1 *A*–*C*) (1, 2). In the bent-closed conformation, the integrin α- and β-subunits bend over at the genu region so that the head and upper legs associate with the lower legs (Fig. 1*A*). In the extended-closed conformation, extension of the α- and β-knees results in separation of the two legs, straightening of the ectodomain, and movement of the headpiece away from the C-terminal domains (Fig. 1*B*). In headpiece opening, conformational change occurs in the ligand-binding site of the βI domain, which is relayed by C-terminal α7-helix pistoning at the hybrid domain interface, and results in swing out of the hybrid domain away from the α-subunit (Fig. 1*C*) (3). The extended-open integrin conformation of $\alpha_L\beta_2$, $\alpha_4\beta_1$, and $\alpha_5\beta_1$ integrins has ∼1,000-fold higher affinity for ligand than the bent-closed and extended-closed conformations (4–6).

Integrin $\alpha_V\beta_6$ binds latent pro-TGF-β1 and -β3 through an Arg-Gly-Asp (RGD)LXX(I/L) motif in the prodomain, and in a cytoskeletal force-dependent mechanism, releases and hence activates TGF-βs (7). Integrins including $\alpha_V\beta_6$ bind ligand at an interface between the β-propeller and βI domains (Fig. 1 *C* and *F*). The Asp sidechain of the ligand binds through its carboxyl group to a Mg^{2+} ion held in the metal ion-dependent adhesion site (MIDAS) of the βI domain (Fig. 1*F*). Two Ca^{2+} ion binding sites flank the MIDAS, one of which is called the adjacent to MIDAS (ADMIDAS). The ADMIDAS metal ion coordinates to the βI domain α1-helix. In opening of the βI domain, the β1–α1 loop and α1-helix with its ADMIDAS metal ion move toward the ligand-binding site and the MIDAS metal ion. In a concerted movement, the βI domain α7-helix pistons and the hybrid domain swings out (Fig. 1 *B*, *C*, *E*, and *F*). Mn^{2+} is commonly used to increase ligand-binding affinity of integrins and is thought to exert its effect by replacing Ca^{2+} at the ADMIDAS (8).

Although the affinity of specific integrin conformational states for ligand and the thermodynamics that regulate the relative stability of these states have been investigated (4–6), the ligand binding kinetics of these conformational states are unknown. We also lack information on how the hybrid domain interface with the βI domain regulates the equilibrium between the closed and open states of the βI domain. Crystal structures of the headpiece of integrin $\alpha_{IIb}\beta_3$ in closed and open states showed that the surface area buried in the βI/hybrid domain interface was larger in the closed than the open conformation. Therefore, it was proposed that the hybrid domain interface stabilizes the βI domain in the closed conformation (3); however, this hypothesis has not yet been tested. This is an important question, because many studies have demonstrated that headpiece opening is the key step in integrin affinity maturation (3–6, 9).

Here, we have characterized the kinetics and affinity of ligand binding by integrin $\alpha_V\beta_6$ on the cell surface or as purified fragments: the ectodomain (clasped or unclasped), headpiece, or headpiece truncated at the hybrid domain, that is, the integrin head (Fig. 1*D*). These studies allow us to understand how different domains contribute to ligand binding affinity and kinetics. The

Significance

Integrins are complex multidomain adhesion molecules. We study how their affinity and binding kinetics for extracellular ligands are regulated, which is essential to enable integrins to communicate with the cytoskeleton. We show that the hybrid domain, which interfaces with the βI domain, strongly regulates affinity for ligand, which binds to a distal face of the βI domain. At high integrin affinity, the ligand binding on-rate goes down. We propose that integrins bind ligand in their low-affinity state, which has a wider ligand-binding pocket, and then convert to their high-affinity state, which has a tighter pocket.

Author contributions: X.D., B.Z., C.L., and T.A.S. designed research; C.L. aided in experiment design and analysis; X.D. and B.Z. performed research; F.-Y.L. and B.N.R. contributed new reagents/analytic tools; and X.D., B.Z., and T.A.S. wrote the paper.

Reviewers: D.S., University of California, San Francisco; J.T., Osaka University; and W.E.E.T., University of Washington.

Conflict of interest statement: T.A.S. owns stock in Morphic Therapeutic.

[1]X.D. and B.Z. contributed equally to this work.

[2]To whom correspondence should be addressed. Email: springer_lab@crystal.harvard.edu.

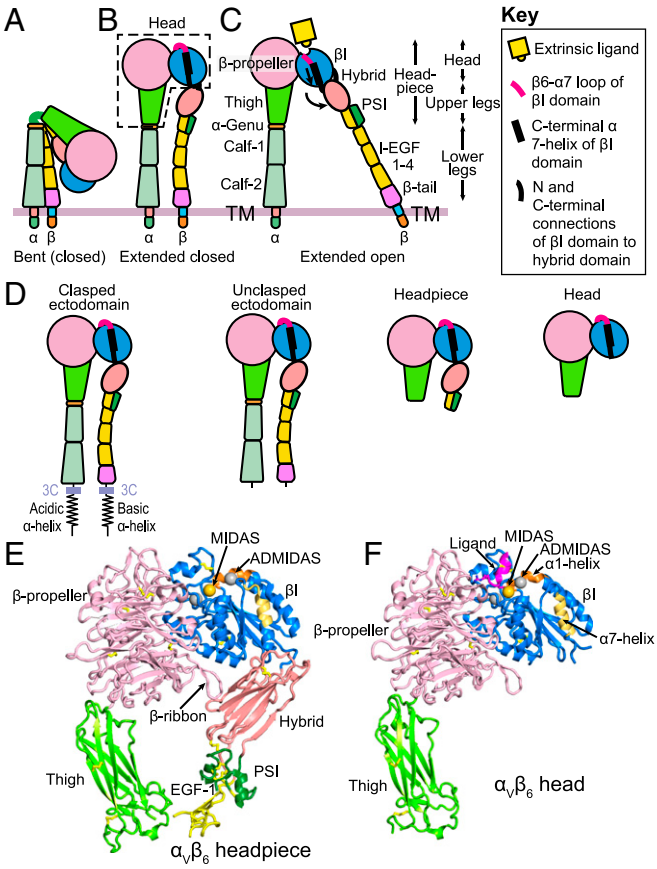

Fig. 1. Integrins. (*A*–*C*) Schematics of the three major integrin conformational states. (*D*) Schematics of soluble $\alpha_V\beta_6$ fragments. A 3C protease site enables clasp removal. (*E* and *F*) Ribbon cartoons of the closed headpiece (*E*) and open head (*F*) of integrin $\alpha_V\beta_6$. The same βI domain residues in each structure are shown in orange (α1-helix) and yellow (α7-helix) to emphasize movements in opening. The three βI-domain metal ions are shown as spheres in gold (MIDAS Mg^{2+}) and silver (Ca^{2+}). The closed headpiece is a model made from PDB ID codes 4UM8 and 4UM9 (17) as described in the Fig. 6 legend and the open head is from PDB ID code 5FFO (7).

$\alpha_V\beta_6$ head has greatly increased affinity and enables insights into kinetics. At high affinity reached by the head in Mn^{2+}, ligand binding on-rate slows, as shown with two different ligands. We relate this finding to the decreased accessibility of the ligand-binding site in the open conformation seen in $\alpha_V\beta_6$ crystal structures (7) and propose a model in which ligand binding to the extended-closed integrin conformation is followed by conversion to the ligand-bound extended-open conformation.

Results

Binding affinity of soluble pro-TGF-β1 for intact integrin $\alpha_V\beta_6$ on the cell surface was measured using fluorescence flow cytometry to measure saturation binding to cells. FITC–pro-TGF-β1 bound to $\alpha_V\beta_6$ on the cell surface with a K_D of 29 nM in 1 mM Mg^{2+}/Ca^{2+} and 3.7 nM in 1 mM Mn^{2+}/0.2 mM Ca^{2+} (Fig. 2 *A* and *B*). We also measured binding affinity in the reverse orientation, using FITC-$\alpha_V\beta_6$ headpiece and transfectants expressing pro-TGF-β1 complexed to GARP on the surface of HEK293 transfectants. FITC-$\alpha_V\beta_6$ headpiece bound to cell surface anchored GARP/pro-TGF-β1 with a K_D of 22 nM in 1 mM Mg^{2+}/Ca^{2+} (Fig. 2*C*) and 6.5 nM in 1 mM Mn^{2+}/0.2 mM Ca^{2+} (Fig. 2 *C* and *D*).

To measure the kinetics of ligand binding, we used surface plasmon resonance (SPR) on immobilized pro-TGF-β1 with soluble, purified, monomeric integrin $\alpha_V\beta_6$ preparations truncated at different positions as analyte. Two types of ectodomain preparations were used, in which the C termini of the integrin α- and β-subunits were connected with a coiled-coil clasp (clasped), or the clasp was proteolytically removed (unclasped, Fig. 1*D*). The clasp, in part, mimics the close association between the ectodomain C termini in the bent-closed conformation (Fig. 1*A*). We used pro-TGF-β1 with an R249A mutation in the proprotein convertase cleavage site. The intact polypeptide linkage between the prodomain and the growth factor in the R249A mutant ensures that the growth factor does not dissociate during regeneration between successive SPR measurements. We were careful to optimize conditions, including gel filtration of integrin fragments to obtain monomeric preparations before SPR, so that binding and dissociation phases at different analyte concentrations (thin black lines, Fig. 3 *A*–*F*) were well fit globally to the 1:1 Langmuir binding model (thicker gray lines, Fig. 3 *A*–*F*).

In Mg^{2+}/Ca^{2+}, the clasped and unclasped ectodomain and headpiece fragments of $\alpha_V\beta_6$ showed K_D and on and off rate values that were within 3-fold of one another (Fig. 3 *A*, *C*, and *G*). In Mg^{2+}/Ca^{2+}, the $\alpha_V\beta_6$ head had a similar on-rate as the longer fragments; however, it showed a markedly lower off-rate and a ∼50-fold higher affinity (inverse K_D) than the headpiece and ectodomain $\alpha_V\beta_6$ fragments (Fig. 3 *E* and *G*).

In Mn^{2+}/Ca^{2+}, off-rate values for the ectodomain and headpiece fragments decreased 25- to 50-fold, and affinity increased by the same amount (Fig. 3 *B*, *D*, and *G*). The k_{on} values of the ectodomain and headpiece fragments in Mn^{2+} were within 1.1-fold of their k_{on} measurements in Mg^{2+} (Fig. 3*G*). In contrast, the k_{on} value for the head decreased 10-fold in Mn^{2+} compared with Mg^{2+}. Furthermore, the dissociation rate constant was too low to be measured (Fig. 3 *F* and *G*). The surprising decrease in k_{on} suggests that at high affinity, when the open conformation of

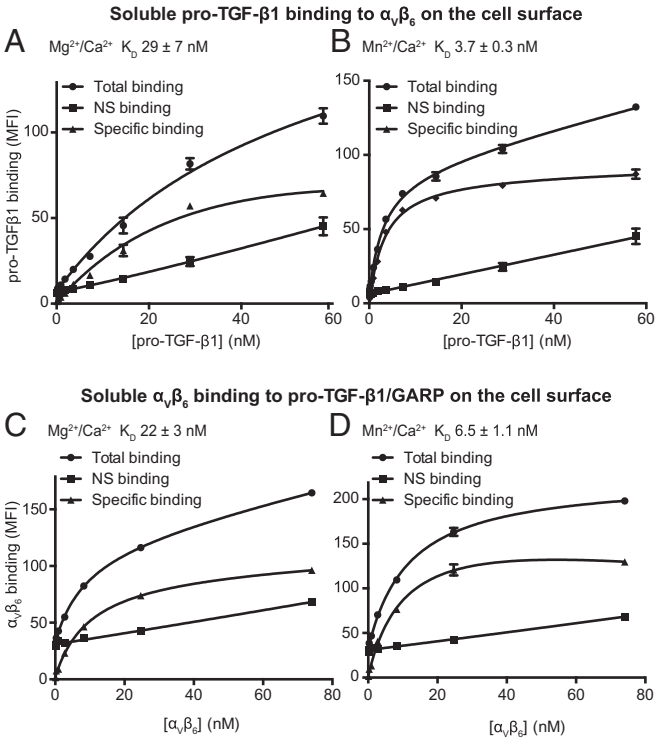

Fig. 2. Saturation binding measured by flow cytometry. (*A* and *B*) Binding of FITC–pro-TGF-β1 to $\alpha_V\beta_6$ transfectants. (*C* and *D*) Binding of FITC-$\alpha_V\beta_6$ headpiece to pro-TGF-β1/GARP transfectants. Binding was in 1 mM Mg^{2+}/1 mM Ca^{2+}, 1 mM Mn^{2+}, and 0.2 mM Ca^{2+}, or 10 mM EDTA. NS, nonspecific binding.

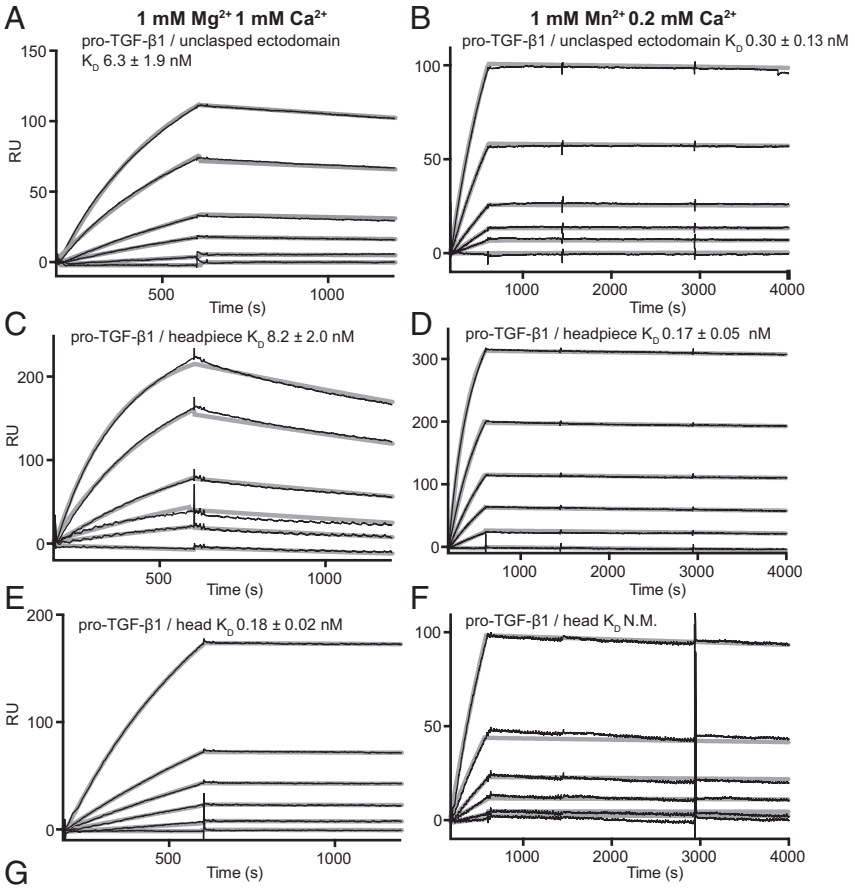

G

pro-TGF-β1	K_D Mg^{2+} (nM)	k_{on} Mg^{2+} (10^4 $M^{-1}s^{-1}$)	k_{off} Mg^{2+} (10^{-4} s^{-1})	K_D Mn^{2+} (nM)	k_{on} Mn^{2+} (10^4 $M^{-1}s^{-1}$)	k_{off} Mn^{2+} (10^{-4} s^{-1})
Clasped ectodomain*	15 ± 9	2.5 ± 1.2	3.3 ± 0.4	0.28 ± 0.03	2.4 ± 0.2	0.068 ± 0.001
Unclasped ectodomain	6.3 ± 1.9	2.4 ± 0.6	1.4 ± 0.1	0.30 ± 0.13	2.1 ± 0.7	0.057 ± 0.008
Headpiece	8.2 ± 2.0	4.2 ± 1.0	3.3 ± 0.1	0.17 ± 0.05	3.9 ± 0.5	0.069 ± 0.010
Head	0.18 ± 0.02	4.2 ± 0.3	0.075 ± 0.003	N.M.	0.42 ± 0.05	N.M.

*Previously published in ref.11

Fig. 3. Kinetics measurements with $\alpha_V\beta_6$ fragments and pro-TGF-β1. (*A–F*) SPR sensorgrams (thin black lines) are shown with fits (thick gray lines). $\alpha_V\beta_6$ fragments and metal ions are indicated. Concentrations used for unclasped integrin $\alpha_V\beta_6$ ectodomain and $\alpha_V\beta_6$ headpiece were 100, 50, 20, 10, 5, and 0 nM in both 1 mM Mg^{2+}/1 mM Ca^{2+} and 1 mM Mn^{2+}/0.2 mM Ca^{2+}. Concentrations used for integrin $\alpha_V\beta_6$ head were 50, 20, 10, 5, 2, and 0 nM in 1 mM Mg^{2+}/1 mM Ca^{2+} and 500, 200, 100, 50, 20, 10, and 0 nM in 1 mM Mn^{2+}/0.2 mM Ca^{2+}. (*G*) K_D and kinetic rates. Values are mean ± difference from mean of two independent experiments. Clasped ectodomain data from ref. 11 are shown for comparison. N.M. not measureable, off-rate is too low.

the βI domain predominates, that $\alpha_V\beta_6$ has slower binding kinetics than at lower affinity, when both closed and open conformational states are present (*Discussion*).

The decrease in k_{on} in Mn^{2+} of the $\alpha_V\beta_6$ head was so striking that we wished to confirm it with another ligand. Thus, we turned to a low-affinity ligand of $\alpha_V\beta_6$ to bring the k_{off} in Mn^{2+} of the $\alpha_V\beta_6$ head into a measurable range. $\alpha_V\beta_6$ recognizes a RGDLXXI/L motif in pro-TGF-β1 and -β3; the Fn3 domain 10 ($Fn3_{10}$) of fibronectin shares the RGD but lacks the LXXI/L of the motif. Kinetic measurements with $Fn3_{9-10}$, $Fn3_{8-10}$, and $Fn3_{7-10}$ fragments of fibronectin gave similar results. Fibronectin fragments bound to the $\alpha_V\beta_6$ head in Mg^{2+} and Mn^{2+} with about 2,000-fold lower affinity than pro-TGF-β1 (Fig. 4 *A* and *B*). The fast headpiece off-rate in Mg^{2+} was difficult to fit accurately (Fig. 4*A*); however, fits to steady-state binding yielded a K_D value within 2-fold of that given by k_{off}/k_{on} (Fig. 4*A*, *Inset*). In Mn^{2+}, affinity of the $\alpha_V\beta_6$ headpiece for fibronectin fragments increased 80-fold (Fig. 4 *B* and *E*). The $\alpha_V\beta_6$ head bound ligands with 50- to 100-fold higher affinity than the headpiece in Mg^{2+}, most of which was due to the slower k_{off} (Fig. 4*E*). In Mn^{2+}, the $\alpha_V\beta_6$ head bound with 5-fold higher affinity than the $\alpha_V\beta_6$ head in Mg^{2+} (Fig. 4 *D* and *E*). Furthermore, in Mn^{2+} the $\alpha_V\beta_6$ head bound with 6-fold higher affinity than the headpiece. Most strikingly, the head k_{on} for fibronectin was decreased 17-fold in Mn^{2+} compared with Mg^{2+}. This decrease in k_{on} was more than compensated by a 107-fold decrease in k_{off} (Fig. 4*E*). In conclusion, kinetics measurements with two different ligands, pro-TGF-β1 and fibronectin fragments, demonstrated a surprising decrease in k_{on} of the $\alpha_V\beta_6$ head in Mn^{2+} compared with Mg^{2+} and compared with the headpiece in Mn^{2+}. Furthermore, the markedly higher affinity of the head than the headpiece demonstrated that the hybrid domain shifts the equilibrium between the closed and open conformations of the β6 βI domain toward the closed conformation, while its deletion shifts the equilibrium toward the open conformation. Shifts in equilibrium do not mean that a single conformational state has been reached. For example, in

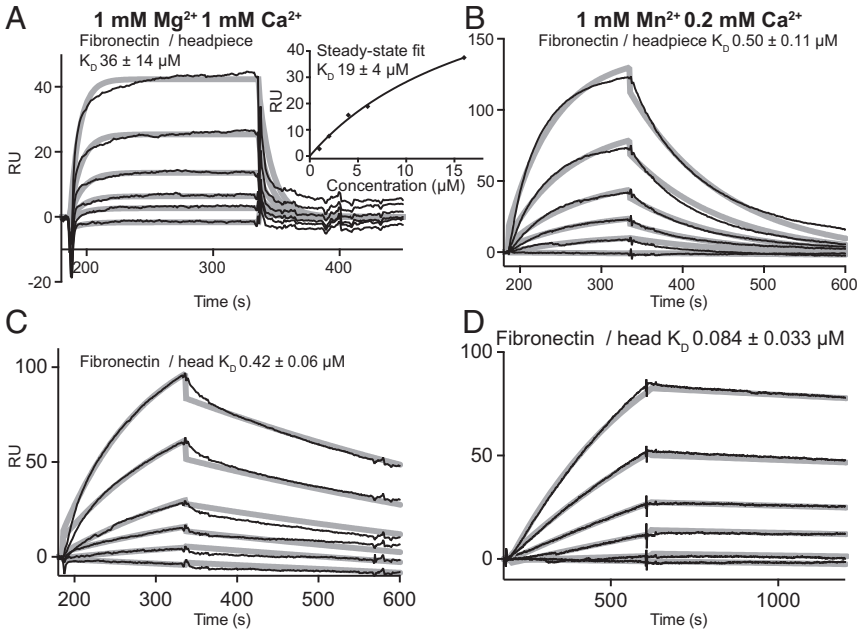

E

Fibronectin	K_D Mg^{2+} (μM)	k_{on} Mg^{2+} (10^3 $M^{-1}s^{-1}$)	k_{off} Mg^{2+} (10^{-3} s^{-1})	K_D Mn^{2+} (μM)	k_{on} Mn^{2+} (10^3 $M^{-1}s^{-1}$)	k_{off} Mn^{2+} (10^{-3} s^{-1})
Headpiece	36 ± 14*	2.6 ± 0.3*	93 ± 34*	0.50 ± 0.11	19 ± 3	9.1 ± 0.2
Head	0.42 ± 0.06	5.7 ± 0.8	2.5 ± 0.2	0.084 ± 0.033	1.1 ± 0.4	0.085 ± 0.009

Fig. 4. Kinetics measurements with $\alpha_V\beta_6$ fragments and fibronectin fragments. (*A–D*) SPR sensorgrams with $Fn3_{8-10}$ (thin black lines) are shown with fits (thick gray lines). $\alpha_V\beta_6$ fragments and metal ions are indicated. (*A*) The $\alpha_V\beta_6$ headpiece concentrations were 16, 8, 4, 2, 1, and 0 μM. *Inset* shows steady-state fit and mean ± SD for three fibronectin fragments. (*B–D*) The $\alpha_V\beta_6$ fragment concentrations were 1,000, 500, 200, 100, 50, and 0 nM. (*E*) K_D and kinetic rates. Values are mean ± SD for one measurement each with $Fn3_{7-10}$, $Fn3_{8-10}$, and $Fn3_{9-10}$, with the exception of the headpiece in Mg^{2+}, for which $Fn3_{7-10}$ and $Fn3_{9-10}$ results could not be fit, and the fit ± fitting error is shown for $Fn3_{8-10}$. *Could not be measured accurately in SPR.

Mg^{2+} the affinity of the head was increased markedly over the headpiece; however, the ability of Mn^{2+} to increase head affinity still further suggested that in Mg^{2+} the head was present in both closed and open conformational states.

To confirm binding affinities by an independent method and gain insights into the thermodynamics of ligand binding by different $\alpha_V\beta_6$ fragments, we used isothermal titration calorimetry (ITC) (Fig. 5). ITC directly measures the enthalpy (ΔH) of receptor-ligand binding; moreover, titrating heat release also measures saturation of receptor–ligand binding and thus also ligand-binding affinity. The K_D values determined for binding of pro-TGF-β1 to the clasped ectodomain, unclasped ectodomain, and headpiece of 20 ± 10, 11 ± 9, and 9.8 ± 4.9 nM, respectively (Fig. 5*E*) by ITC were within error of those measured by SPR of 15 ± 9, 6.3 ± 1.9, and 8.2 ± 2.0 nM, respectively (Fig. 3*G*). The affinity of the head for pro-TGF-β1 was too high to be measured by ITC and therefore we used ΔH from ITC and ΔG derived from affinity measured by SPR to calculate the entropy ΔS of binding.

The free energy of ligand binding is given by $\Delta G = \Delta H - T\Delta S$; therefore, we report $-T\Delta S$ at 298 K in Fig. 5*E*. All measurements were in 1 mM Mg^{2+}/1 mM Ca^{2+}. ΔH and $-T\Delta S$ values for the clasped and unclasped ectodomains were very similar and showed that a large enthalpy of binding of approximately −19 kcal/mol overcame an entropy decrease with a $-T\Delta S$ term of ∼8 kcal/mol (Fig. 5*E*). Interestingly, headpiece binding to pro-TGF-β1 was favored by both enthalpy and entropy, with large compensating decreases in enthalpy and increases in entropy relative to the ectodomain fragments (Fig. 5*E*). Thus, the lower legs play an important role in the thermodynamics of ligand binding. Truncation of the headpiece to the head markedly altered the thermodynamics of pro-TGF-β1 binding. Compared with the headpiece, binding to the head was driven by a large increase in enthalpy and opposed by a small decrease in entropy with a positive $-T\Delta S$ term (Fig. 5*E*).

Discussion

Studies here provide insights into the molecular components of $\alpha_V\beta_6$ integrin that regulate its affinity for ligand, and results with a head fragment in Mn^{2+} reveal a surprising slowing of ligand binding kinetics when $\alpha_V\beta_6$ reaches high affinity. We place our results in the context of recent thermodynamic studies on β_1 integrins that have shown how ligand-binding affinities are regulated by integrin conformational change. Studies on $\alpha_4\beta_1$ and $\alpha_5\beta_1$ showed that affinities of their open conformations were 5,000-fold ($\alpha_5\beta_1$) and 700-fold ($\alpha_4\beta_1$) higher than their closed conformations and that these affinities were intrinsic, that is, independent of whether the conformation was on the cell surface or in a particular integrin fragment (5, 6, 10). Differences in affinities among cell-surface integrins and different integrin fragments were caused by differences in relative free energies of conformational states (and their populations) within ensembles in each type of integrin preparations. To a very good approximation, affinity was proportional to the percentage of the open conformation in each preparation.

Integrins $\alpha_4\beta_1$, $\alpha_5\beta_1$, and $\alpha_V\beta_6$ all appear to have bent-closed, extended-closed, and extended-open conformations. This conclusion is directly demonstrated for $\alpha_5\beta_1$ and $\alpha_V\beta_6$ by EM (10, 11) and may be inferred for $\alpha_4\beta_1$ by the effects of Fabs that stabilize the closed, open, and extended states on affinity of soluble $\alpha_4\beta_1$ fragments for ligands and $\alpha_4\beta_1$-dependent cell adhesion to specific ligand (6). We therefore interpret the increase in $\alpha_V\beta_6$ affinity

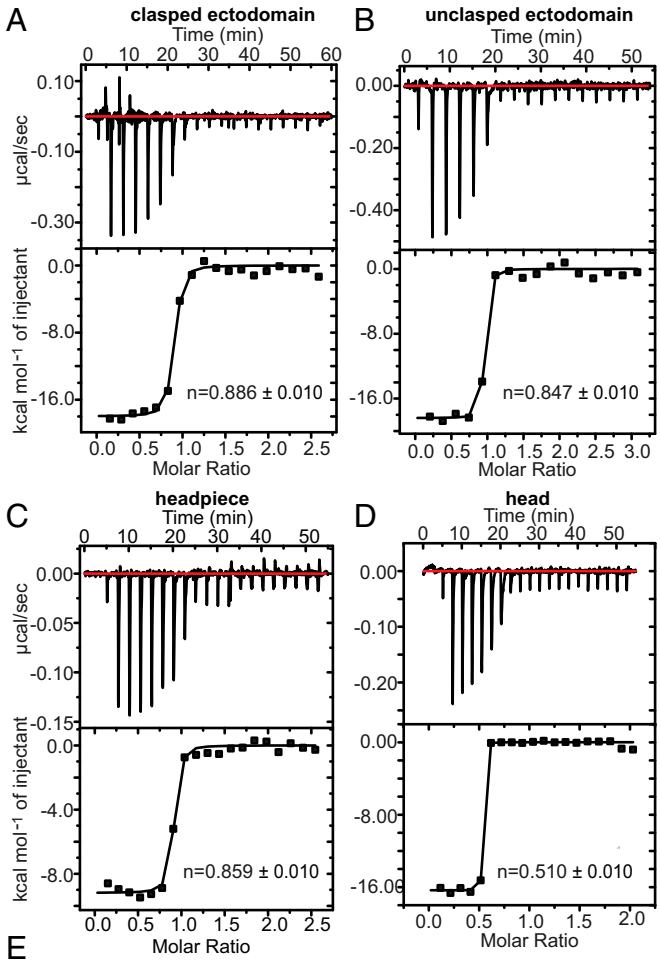

E

αVβ6	K_D (nM)	ΔH (kcal/M)	-TΔS (kcal/M)
Clasped ectodomain	19.7 ± 10.3	-18.5 ± 0.5	8.05 ± 0.84
Unclasped ectodomain	10.7 ± 8.8	-18.6 ± 0.5	7.8 ± 1.2
Headpiece	9.8 ± 4.9	-9.2 ± 0.2	-1.67 ± 0.47
Head	0.182 ± 0.020*	-16.3 ± 0.15	3.09 ± 0.21*

Fig. 5. Thermodynamics of $\alpha_V\beta_6$ fragment binding to pro-TGF-β1 measured with ITC in 1 mM Mg^{2+} and 1 mM Ca^{2+}. (*A–D*) Data are shown for the indicated constructs. (*E*) Affinity and thermodynamics. Values are shown ± fitting error from Origin 7. *Affinity was too high to be measured by ITC; K_D was taken from SPR and used to calculate TΔS.

seen with truncation of the hybrid domain and addition of Mn^{2+} as an increase in the proportion of the open headpiece conformation in the $\alpha_V\beta_6$ conformational ensemble. Compared with the clasped ectodomain, the head $\alpha_V\beta_6$ fragment showed an 80-fold increase in affinity in Mg^{2+}. With its extremely slow off-rate, the affinity for pro-TGF-β1 of the $\alpha_V\beta_6$ head in Mn^{2+} was too high for measurement by SPR. However, we were able to measure the increase in affinity for fibronectin of the $\alpha_V\beta_6$ head in Mn^{2+} compared with Mg^{2+} as 5-fold. Multiplying the 80-fold by the 5-fold increase in affinity yields a 400-fold increase in affinity. We assume that both open and closed conformational states are present in the clasped ectodomain basal ensemble, and thus 400-fold is an estimate of the minimum increase in affinity to be expected between the closed and open conformations of integrin $\alpha_V\beta_6$. This value is not too far removed from the difference in intrinsic affinity measured for the open and closed conformations of 700-fold for $\alpha_4\beta_1$ and 5,000-fold for $\alpha_5\beta_1$ (5, 6, 10).

For both $\alpha_4\beta_1$ and $\alpha_5\beta_1$, the population of the closed and open conformations in ensembles regulates ensemble affinity, while intrinsic affinity of the closed and open states is independent of whether integrin legs or clasp are present, whether the integrin is a soluble fragment or on the cell surface, or other features such as glycosylation (5, 6). Nonetheless, the influence of particular segments such as the lower legs on the population of the states (their relative stabilities) was found to vary significantly for $\alpha_4\beta_1$ and $\alpha_5\beta_1$. Our results here suggest further differences with $\alpha_V\beta_6$. Affinity for pro-TGF-β1 of $\alpha_V\beta_6$ on intact cells and $\alpha_V\beta_6$ soluble clasped or unclasped ectodomain or headpiece fragments differed by no more than 4-fold. These results were strengthened by flow cytometry measurements of pro-TGF-β1 and $\alpha_V\beta_6$ headpiece binding to intact $\alpha_V\beta_6$ and intact pro-TGF-β1–GARP complexes on cell surfaces, respectively, that showed only 2-fold differences in affinity. For $\alpha_4\beta_1$, the presence of the lower legs only modestly increased ensemble affinity, by 5-fold. In contrast, the lower legs of $\alpha_5\beta_1$ appeared to strongly repel one another when they were close together in the closed conformation; the presence of the lower legs in $\alpha_5\beta_1$ increased the affinity of the ectodomain compared with the headpiece by 80-fold. In $\alpha_V\beta_6$, lower leg truncation had little effect on affinity. Thus, the effect of the lower legs on the open/closed conformational equilibrium is highly variable among integrins $\alpha_4\beta_1$, $\alpha_5\beta_1$, and $\alpha_V\beta_6$, with the difference between $\alpha_4\beta_1$ and $\alpha_5\beta_1$ (16-fold) being greater than between $\alpha_4\beta_1$ and $\alpha_V\beta_6$. Integrins $\alpha_4\beta_1$ and $\alpha_5\beta_1$ showed a 90- and 280-fold decrease in affinity on the cell surface compared with soluble ectodomains, respectively, whereas $\alpha_V\beta_6$ showed only a 2- to 4-fold decrease. The transmembrane and cytoplasmic domains and cellular environment thus stabilize the closed conformations much more for $\alpha_4\beta_1$ and $\alpha_5\beta_1$ integrins than for $\alpha_V\beta_6$. The structural basis for differences in relative stabilities of cell surface and soluble forms could reflect differences between cytoplasmic domains and their association with cytoplasmic adaptor proteins, differences between the α- and β-subunit transmembrane domains and the strength of their association with one another, or differences in the length of the linkers that connect the last extracellular domain in each subunit to the transmembrane domain. Lengthening linkers increases basal integrin activity on the cell surface (12, 13); however, the length of the linkers is identical in the α_5 and α_V subunits and in the β_1 and β_6 subunits. The C-terminal portion of the β_6 transmembrane domain contains a cysteine residue; however, there is no evidence that it is palmitylated. Further work is required to understand the small contribution of membrane embedding on the basal ensemble affinity of $\alpha_V\beta_6$ relative to $\alpha_4\beta_1$ and $\alpha_5\beta_1$ integrins. However, it should be pointed out that our estimate that maximally activated $\alpha_V\beta_6$ increases in affinity ∼400-fold relative to cell surface or clasped ectodomain $\alpha_V\beta_6$ implies that on the cell surface, ∼0.25% of $\alpha_V\beta_6$ is in the extended-open conformation. Similarly, $\alpha_4\beta_1$ and $\alpha_5\beta_1$ integrins are 0.3–0.9% and 0.1–0.2% extended-open, respectively, on different cell types (6). Thus, these three integrins appear similar to one another in their need for activation on cell surfaces and differ most energetically as soluble fragments.

Although we found that $\alpha_V\beta_6$ headpiece and ectodomain fragments had similar affinities, ITC measurements showed that enthalpy and entropy made very different contributions to stabilizing the ectodomain and headpiece. The presence of the lower legs decreased ΔH by ∼10 kcal/mol and increased −TΔS by a similar amount in the ectodomain compared with the headpiece. Ligand binding to the headpiece was driven by both enthalpy and entropy. In contrast, ligand binding to the head was greatly favored enthalpically and moderately disfavored entropically. Thermodynamics also confirmed our SPR measurements

of $\alpha_V\beta_6$ clasped and unclasped ectodomain and headpiece fragment affinity for pro-TGF-β1.

Overall, these results reveal major differences in the way in which important structural components in integrins, including the transmembrane/cytoplasmic domains and lower legs, regulate ligand-binding affinity by the integrin head. Recent studies on integrin $\alpha_V\beta_8$ also revealed only a four- to fivefold difference in affinity among clasped and unclasped ectodomain and headpiece forms (11). However, $\alpha_V\beta_8$ exists only in the closed conformation (11, 14) and therefore is not comparable to $\alpha_V\beta_6$, $\alpha_4\beta_1$, or $\alpha_5\beta_1$, all of which have both closed and open conformations. Both $\alpha_V\beta_6$ and $\alpha_V\beta_8$ are specialized for activation of TGF-β1; it would be interesting to determine whether differences from $\alpha_4\beta_1$ and $\alpha_5\beta_1$ in $\alpha_V\beta_6$ affinity regulation also hold for integrins $\alpha_V\beta_1$, $\alpha_V\beta_3$, and $\alpha_V\beta_5$, or are limited to $\alpha_V\beta_6$ and $\alpha_V\beta_8$.

The interface between the βI and hybrid domains completely rearranges during opening of the βI domain. βI domain opening is linked to swing out of the hybrid domain, which results in a decrease in buried solvent-accessible surface area on each side of the interface from 1,020 Å^2 in the closed state to 750 Å^2 in the open state in integrin $\alpha_{IIb}\beta_3$ structures Protein Data Bank (PDB) ID codes 3T3P (15) and 2VDR (16). These results confirm an earlier comparison between closed integrin $\alpha_V\beta_3$ and open integrin $\alpha_{IIb}\beta_3$ (3). Since greater buried surface area correlates with increased stability of protein–protein interfaces, it was previously hypothesized that the interface with the hybrid domain stabilizes the βI domain in the closed conformation (3).

The hybrid domain in $\alpha_V\beta_6$ not only interfaces with the βI domain, but also contacts a long β-ribbon in the β-propeller domain in a hydrophilic interface (Fig. 1*E*). Such long β-ribbons between the β2 and β3 strands in β-propeller β-sheet 5 are also present in the integrin α_V, α_5, and α_{IIb} subunits. β-Ribbon contacts with the hybrid domain bury solvent accessible surface area on each side of the interface of 310 Å^2 in $\alpha_V\beta_6$ (17), 100 Å^2 in $\alpha_V\beta_3$ (18), 80 Å^2 in $\alpha_{IIb}\beta_3$ (15), and 140 Å^2 in $\alpha_5\beta_1$ (19). The hybrid domain swings away from the α-subunit in the open conformation, and β-ribbon contacts are not present in open headpiece structures. Since the hybrid domain interfaces with the βI domain and β-propeller β-ribbon are each abolished by deletion of the hybrid domain, our study does not discriminate between which interface is more important in the observed increase in affinity and hypothesized shift in equilibrium toward the open conformation. Only integrin α-subunits in the RGD-binding α-subunit subfamily have long β2–β3 loops in β-propeller β-sheet 5, and crystal structures of integrins in other subfamilies including $\alpha_X\beta_2$, $\alpha_L\beta_2$, and $\alpha_4\beta_7$ show no contacts between the β-propeller and hybrid domains (20–22). Studies on a large number of integrin headpiece constructs, including those with short β2–β3 loops in β-propeller β-sheet 5, that is, integrins $\alpha_X\beta_2$, $\alpha_L\beta_2$, $\alpha_M\beta_2$, $\alpha_4\beta_7$, and $\alpha_4\beta_1$, show that the conformational equilibrium is strongly biased to the closed over the open conformation (2, 6, 20, 21, 23). Accordingly, it is likely that the βI-hybrid domain interface is more important than the hydrophilic contact with the β-propeller β-ribbon in the increase in affinity of the head construct observed here.

The hybrid domain was the most important component of integrin molecular structure identified in this paper for regulating $\alpha_V\beta_6$ ligand-binding affinity. Deletion of the hybrid domain resulted in a 50-fold increase in affinity for pro-TGF-β1 of the $\alpha_V\beta_6$ head compared with the headpiece. We were fortunate to be able to express the $\alpha_V\beta_6$ head construct. We failed to obtain secretion from mammalian cell lines transfected with similar head constructs for integrins $\alpha_4\beta_1$, $\alpha_5\beta_1$, $\alpha_{IIb}\beta_3$, and $\alpha_V\beta_8$. The $\alpha_V\beta_6$ head construct is stabilized by an engineered disulfide bond between the β-propeller and βI domains (17). However, even with a similar disulfide in $\alpha_V\beta_8$ that enables good $\alpha_V\beta_8$ headpiece expression (11), the $\alpha_V\beta_8$ head construct failed to express.

The $\alpha_V\beta_6$ head protein allowed us to observe a most interesting phenomenon: as ligand-binding affinity reached high levels, k_{on} underwent a sudden decrease. Over a 90-fold range in affinity, the k_{on} for pro-TGF-β1 was steady within a 2-fold range for ectodomain and headpiece preparations in Mg^{2+} and Mn^{2+} and the head in Mg^{2+}. In contrast, head k_{on} in Mn^{2+} decreased 10-fold compared with head k_{on} in Mg^{2+} and headpiece k_{on} in Mn^{2+}. To test this result with a distinct ligand, we turned to low-affinity fibronectin fragments containing the RGD motif in the $Fn3_{10}$ domain. We confirmed our observation by demonstrating a 5.2-fold decrease in k_{on} for the head in Mn^{2+} compared with Mg^{2+}, and a 17-fold decrease in k_{on} in Mn^{2+} for the head compared with the headpiece.

Our results clearly demonstrate that when $\alpha_V\beta_6$ reaches a sufficiently high affinity for ligand, its ligand-binding on-rate decreases. We discuss these results in terms of the closed and open conformations of the $\alpha_V\beta_6$ βI domain, head, headpiece, and ectodomain, which have been variously observed in crystal structure and electron microscopy studies that have demonstrated the high affinity of the open state (7, 11, 17). We use concepts derived from measurements of the affinity intrinsic to integrin conformational states and the conformational equilibria between states (5, 6). Using values for $\alpha_5\beta_1$ and $\alpha_4\beta_1$, we estimate that the open $\alpha_V\beta_6$ conformation has 1,000-fold higher affinity than the closed conformation. Therefore, the increase in affinity in Mn^{2+} compared with Mg^{2+} of 20- to 50-fold seen with ectodomain and headpiece binding to pro-TGF-β1 suggests a similar 20- to 50-fold increase in the population of the open conformation in the conformational state ensemble. Notably, head affinity for fibronectin increased markedly less in Mn^{2+} compared with Mg^{2+}, by 5-fold. This nonproportionality is exactly what is expected if in contrast to the headpiece in Mn^{2+} and the head in Mg^{2+}, the head in Mn^{2+} is nearing saturable population of the open conformation. Thus, we believe that the open conformation of the head is approaching 100% population in Mn^{2+}, and that k_{on} is approaching that of the open $\alpha_V\beta_6$ conformation. In all other conditions, affinity was at least 5-fold lower, and thus the closed conformation would be in >4-fold excess over the open conformation. In these lower-affinity conditions, the closed conformation on-rate, if higher than that of the open conformation, would be expected to dominate. This model fits experimental observations well. The ligand-bound open conformation could then accumulate by conversion from the ligand-bound closed conformation. Crystallographic experiments have clearly established that ligand can bind to the closed integrin conformation and induce the open conformation (9). The $\alpha_V\beta_6$ headpiece crystallizes in the closed conformation in absence of ligand; soaking ligand into crystals induced conversion to an intermediate conformation; full headpiece opening was blocked by contacts in the crystal lattice (17). While we have clearly observed that on-rate decreases at high $\alpha_V\beta_6$ affinity, we have no direct evidence for interpretation of kinetic results in terms of closed and open conformations. Direct evidence could come from Fabs that stabilize specific integrin conformational states, but these are currently lacking for $\alpha_V\beta_6$, in contrast to β_1 integrins (5, 6, 10).

Our results suggest that both closed and open integrin conformations have important functions in ligand binding. Integrin binding to ligand may be kinetically more favored for closed conformations, and especially for the extended-closed conformation, which has a ligand-binding site with greater accessibility for extracellular ligands (Fig. 1 *A–C*). Once the extended-closed conformation binds ligand, rapid conversion could occur to the extended-open conformation, with its high affinity and slower k_{off}. When integrins on cells bind ligands on substrates, tensile force is applied to integrin cytoplasmic domains by the actin cytoskeleton (24, 25). Such force, together with the much higher

affinity of the open conformation for ligand, strongly stabilizes integrins in the extended-open conformation (26).

Rapid binding to low-affinity states, followed by conversion to high-affinity states, is an emerging finding for several classes of adhesion molecules. Selectins have tandem N-terminal lectin and EGF domains with two conformational states, bind glycoprotein ligands containing sialyl Lewis^X, and mediate transient rolling adhesion of leukocytes on vessel walls in shear flow. A mutation that stabilized the high-affinity state was found to decrease on-rate as well as off-rate, increase affinity, stabilize selectin adhesiveness and resistance to detachment by increased shear flow, and to slow the velocity of rolling cells (27). FimH is a bacterial adhesin with an N-terminal lectin domain that has two conformational states and binds mannose. FimH is expressed on the tips of pili and enables *Escherichia coli* to bind to host cells in shear flow. Mutations that stabilize the high-affinity state of FimH increase ligand binding under static conditions but markedly slow on-rate and bind less efficiently in shear flow (28). Selectins, FimH, and integrins all have high-affinity conformations that are more extended than their low-affinity conformations, and thus tensile force applied when ligand is bound stabilizes the high-affinity state. All three classes of adhesion molecules function in settings in which they must resist substantial applied force, which simultaneously both stabilizes their high-affinity states and destabilizes their receptor-ligand bonds. In all cases, it appears that the low-affinity state may have an important biological function by allowing rapid binding to ligand, with subsequent ligand binding-induced conversion to the high-affinity state, which is further stabilized by applied tensile force.

In change from the closed to the open conformation of integrin $\alpha_V\beta_6$, the ligand-binding pocket tightens up, immediately suggesting a structural basis for a decrease in ligand-binding on-rate and also a potential mechanism for increased force resistance (Fig. 6). The MIDAS Mg^{2+} ion to which the RGD Asp carboxyl group binds lies at the bottom of the ligand-binding pocket and is much better exposed in the closed than open conformation. Inward movement of the β1–α1 loop in the open conformation partially occludes the MIDAS and markedly decreases the diameter of the binding pocket for the Asp sidechain (Fig. 6). The binding geometry of the Asp carboxyl group also becomes highly constrained in the open conformation by two hydrogen bonds that form backbone NH groups in the β1–α1 loop after it moves inward and complement carboxyl oxygen coordination with the MIDAS Mg^{2+} ion (7). These spatial and geometric constraints limit ligand access to the pocket in the open conformation and are expected to decrease on-rate. These and other changes upon opening are also expected to decrease off-rate and to be responsible for the ∼1,000-fold increase in affinity of the open compared with the closed integrin conformation.

Materials and Methods

Soluble $\alpha_V\beta_6$ ectodomains, headpiece, and head were prepared as in ref. 7. Proteins were expressed in HEK293S Gnt I$^-$ cells with Ex-Cell 293 serum-free media (Sigma). For purification, culture supernatant was first passed through a Ni-NTA affinity column (Qiagen). Proteins were cleaved with 3C protease at 4 °C overnight and further purified using ion exchange (Q Fast-Flow Sepharose, GE Healthcare) at pH 8.0 with a NaCl gradient from 50 mM to 1 M and finally gel filtration (Superdex 200, GE Healthcare). Human pro-TGF-β1 R249A mutant protein expression and purification were as described (7). Fibronectin fragments containing $Fn3_{7-10}$ (mature residues 1,142–1,509), $Fn3_{8-10}$ (mature residues 1,233–1,509), and $Fn3_{9-10}$ (mature residues 1,326–1,509) were expressed in *E. coli* and purified as described (29, 30).

For flow cytometry (7, 17), wild-type α_V in a modified pEF1 vector and β_6 in pcDNA3.1(–) vector were transiently cotransfected into 293T cells using Lipofectamine 2000 (Life Technologies). Transfectants were incubated with FITC–pro-TGF-β1 in 20 mM Hepes, 5 mM KCl, 5.5 mM glucose, 137 mM NaCl,

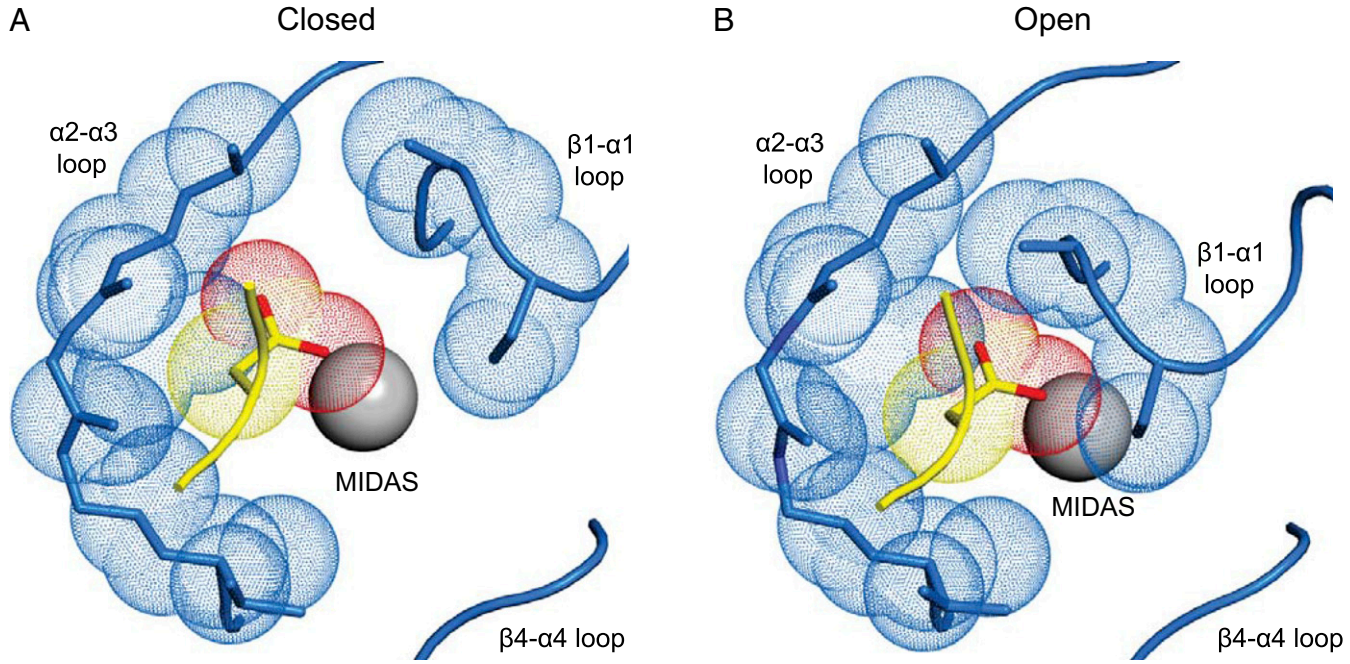

Fig. 6. The binding pocket in the βI domain of integrin $\alpha_V\beta_6$ for the Asp sidechain of the pro-TGF-β RGD motif. (*A*) Liganded closed conformation. (*B*) Liganded open conformation. The pocket in the β_6 βI domain is shown with backbone and close-by sidechains in blue stick and the MIDAS Mg^{2+} ion as a silver sphere. Pocket atoms that are close to the ligand in the open conformation are shown as blue dot surfaces. The ligand Asp sidechain and its loop are shown in stick and worm trace in yellow, except the Asp sidechain carboxyl oxygens are red. The Asp sidechain Cβ and Cγ carbons and carboxyl oxygens are shown as yellow and red dot surfaces, respectively. *A* is a model of liganded, closed $\alpha_V\beta_6$ made from two structures (17). PDB ID code 4UM8 is closed, but lacks a bound ligand and its MIDAS Mg^{2+} ion is displaced because a neighboring Ca^{2+} ion is missing. PDB ID code 4UM9 contains a soaked-in TGF-β3 peptide and all βI-domain metal ions, but as a consequence of ligand binding, the β1–α1 loop has moved toward the open conformation into an intermediate conformation. Therefore, the model uses 4UM9 except the β1–α1 loop and ADMIDAS Ca^{2+} ions are from 4UM8. *B* is from the open $\alpha_V\beta_6$ head bound to pro-TGF-β1 (PDB ID code 5FFO) (7).

1% BSA containing 1 mM Mg^{2+}/1 mM Ca^{2+}, 1 mM Mn^{2+}/0.2 mM Ca^{2+}, or 10 mM EDTA at room temperature for 30 min and subjected to flow cytometry without washing. Mean fluorescence intensity (MFI) was reported with or without subtraction of nonspecific binding in EDTA. Similarly, wild-type pro-TGF-β1 in pcDNA3.1(–) vector and GARP in pLEXm vector were transiently cotransfected into 293T cells using Lipofectamine 2000. Transfectants were incubated with FITC-$\alpha_V\beta_6$ under the same conditions and binding measured as described above.

For SPR using Biacore 3000 (GE Healthcare), purified pro-TGF-β1 R249A furin site mutant or fibronectin fragments were amine immobilized on a CM5 chip. Soluble $\alpha_V\beta_6$ fragments were gel filtered using Superdex 200 to remove aggregates before use. Protein was injected at 20 μL/min in 0.15 M NaCl, 20 mM Hepes pH 7.4 with indicated metal ions. The surface was regenerated with a 10- to 60-s pulse of 25 mM HCl at the end of each cycle to restore resonance units to baseline. Kinetics and affinity analysis were performed with SPR evaluation software version 4.0.1 (GE Healthcare).

For ITC, proteins were dialyzed overnight against 150 mM NaCl, 20 mM Tris·HCl pH 7.4, 1 mM $MgCl_2$, 1 mM $CaCl_2$, degassed, and centrifuged at 20,000 × *g* for 10 min. Integrin (100 μM) was titrated into 10 μM pro-TGF-β1 in a MicroCal iTC200 (GE Healthcare Life Sciences). A priming injection of 0.4 μL (not included in data analysis) was followed by 2-μL injections every 180 s. Data averaged over 2-s windows were analyzed using Origin 7.

ACKNOWLEDGMENTS. We thank Jing Li for her critical reading of the manuscript and Siavash Mostafavi and Eugene Nebelitsky for protein purification. This work was supported by NIH Grant AR-067288.

1. Luo B-H, Carman CV, Springer TA (2007) Structural basis of integrin regulation and signaling. *Annu Rev Immunol* 25:619–647.
2. Springer TA, Dustin ML (2012) Integrin inside-out signaling and the immunological synapse. *Curr Opin Cell Biol* 24:107–115.
3. Xiao T, Takagi J, Coller BS, Wang JH, Springer TA (2004) Structural basis for allostery in integrins and binding to fibrinogen-mimetic therapeutics. *Nature* 432:59–67.
4. Schürpf T, Springer TA (2011) Regulation of integrin affinity on cell surfaces. *EMBO J* 30:4712–4727.
5. Li J, et al. (2017) Conformational equilibria and intrinsic affinities define integrin activation. *EMBO J* 36:629–645.
6. Li J, Springer TA (2018) Energy landscapes differences among integrins establish the framework for understanding activation. *J Cell Biol* 217:397–412.
7. Dong X, et al. (2017) Force interacts with macromolecular structure in activation of TGF-β. *Nature* 542:55–59.
8. Chen J, Salas A, Springer TA (2003) Bistable regulation of integrin adhesiveness by a bipolar metal ion cluster. *Nat Struct Biol* 10:995–1001.
9. Zhu J, Zhu J, Springer TA (2013) Complete integrin headpiece opening in eight steps. *J Cell Biol* 201:1053–1068.
10. Su Y, et al. (2016) Relating conformation to function in integrin α5β1. *Proc Natl Acad Sci USA* 113:E3872–E3881.
11. Wang J, et al. (2017) Atypical interactions of integrin αVβ8 with pro-TGF-β1. *Proc Natl Acad Sci USA* 114:E4168–E4174.
12. Xiong YM, Chen J, Zhang L (2003) Modulation of CD11b/CD18 adhesive activity by its extracellular, membrane-proximal regions. *J Immunol* 171:1042–1050.
13. Zhu J, et al. (2009) The structure of a receptor with two associating transmembrane domains on the cell surface: Integrin $\alpha_{IIb}\beta_3$. *Mol Cell* 34:234–249.
14. Minagawa S, et al. (2014) Selective targeting of TGF-β activation to treat fibroinflammatory airway disease. *Sci Transl Med* 6:241ra79.
15. Zhu J, et al. (2012) Structure-guided design of a high-affinity platelet integrin αIIbβ3 receptor antagonist that disrupts Mg^{2+} binding to the MIDAS. *Sci Transl Med* 4: 125ra32.
16. Springer TA, Zhu J, Xiao T (2008) Structural basis for distinctive recognition of fibrinogen gammaC peptide by the platelet integrin alphaIIbbeta3. *J Cell Biol* 182: 791–800.
17. Dong X, Hudson NE, Lu C, Springer TA (2014) Structural determinants of integrin β-subunit specificity for latent TGF-β. *Nat Struct Mol Biol* 21:1091–1096.
18. Dong X, et al. (2012) $\alpha_V\beta_3$ integrin crystal structures and their functional implications. *Biochemistry* 51:8814–8828.
19. Xia W, Springer TA (2014) Metal ion and ligand binding of integrin $\alpha_5\beta_1$. *Proc Natl Acad Sci USA* 111:17863–17868.
20. Sen M, Springer TA (2016) Leukocyte integrin αLβ2 headpiece structures: The αI domain, the pocket for the internal ligand, and concerted movements of its loops. *Proc Natl Acad Sci USA* 113:2940–2945.
21. Yu Y, et al. (2012) Structural specializations of $\alpha_4\beta_7$, an integrin that mediates rolling adhesion. *J Cell Biol* 196:131–146.
22. Xie C, et al. (2010) Structure of an integrin with an αI domain, complement receptor type 4. *EMBO J* 29:666–679.
23. Xu S, Wang J, Wang JH, Springer TA (2017) Distinct recognition of complement iC3b by integrins αXβ2 and αMβ2. *Proc Natl Acad Sci USA* 114:3403–3408.
24. Chang AC, et al. (2016) Single molecule force measurements in living cells reveal a minimally tensioned integrin state. *ACS Nano* 10:10745–10752.
25. Nordenfelt P, Elliott HL, Springer TA (2016) Coordinated integrin activation by actin-dependent force during T-cell migration. *Nat Commun* 7:13119.
26. Li J, Springer TA (2017) Integrin extension enables ultrasensitive regulation by cytoskeletal force. *Proc Natl Acad Sci USA* 114:4685–4690.
27. Phan UT, Waldron TT, Springer TA (2006) Remodeling of the lectin-EGF-like domain interface in P- and L-selectin increases adhesiveness and shear resistance under hydrodynamic force. *Nat Immunol* 7:883–889.
28. Yakovenko O, Tchesnokova V, Sokurenko EV, Thomas WE (2015) Inactive conformation enhances binding function in physiological conditions. *Proc Natl Acad Sci USA* 112:9884–9889.
29. Leahy DJ, Aukhil I, Erickson HP (1996) 2.0 Å crystal structure of a four-domain segment of human fibronectin encompassing the RGD loop and synergy region. *Cell* 84: 155–164.
30. Takagi J, Erickson HP, Springer TA (2001) C-terminal opening mimics 'inside-out' activation of integrin $\alpha_5\beta_1$. *Nat Struct Biol* 8:412–416.